Applied Physics Letters

Performance enhancement of a self-powered solar-blind UV photodetector based on $ZnGa_2O_4$/Si heterojunction via interface pyroelectric effect

Cite as: Appl. Phys. Lett. **118**, 251101 (2021); https://doi.org/10.1063/5.0049747
Submitted: 08 March 2021 • Accepted: 03 June 2021 • Published Online: 21 June 2021

Dongyang Han, Kewei Liu, Xing Chen, et al.

Applied Physics Letters ARTICLE scitation.org/journal/apl

Performance enhancement of a self-powered solar-blind UV photodetector based on $ZnGa_2O_4$/Si heterojunction via interface pyroelectric effect

Cite as: Appl. Phys. Lett. **118**, 251101 (2021); doi: 10.1063/5.0049747
Submitted: 8 March 2021 · Accepted: 3 June 2021 ·
Published Online: 21 June 2021

View Online Export Citation CrossMark

Dongyang Han,[1,2] Kewei Liu,[1,2,a)] Xing Chen,[1,2] Binghui Li,[1,2] Tianyou Zhai,[3] Lei Liu,[1,2] and Dezhen Shen[1,2,a)]

AFFILIATIONS

[1]State Key Laboratory of Luminescence and Applications, Changchun Institute of Optics, Fine Mechanics and Physics, Chinese Academy of Sciences, Changchun 130033, People's Republic of China
[2]Center of Materials Science and Optoelectronics Engineering, University of Chinese Academy of Sciences, Beijing 100049, People's Republic of China
[3]State Key Laboratory of Materials Processing and Die & Mould Technology, School of Materials Science and Engineering, Huazhong University of Science and Technology (HUST), Wuhan 430074, People's Republic of China

[a)]**Authors to whom correspondence should be addressed:** liukw@ciomp.ac.cn and shendz@ciomp.ac.cn

ABSTRACT

The photodetectors based on the wide bandgap semiconductor (WBS)/Si heterojunction have attracted more and more attention in recent years due to their excellent photoelectric characteristics and easy integration capabilities. In this work, we have demonstrated a self-powered solar-blind ultraviolet (UV) photodetector based on the $ZnGa_2O_4$/Si heterojunction. A typical rectification characteristic with a rectification ratio exceeding 10^3 within ±5 V can be obtained. At 0 V bias, the −3 dB cutoff wavelength of ∼255 nm and the UV-visible rejection ratio of $\sim 3 \times 10^2$ show that the device has excellent self-powered solar-blind UV detection performance. In addition, the responsivity and the response speed of $ZnGa_2O_4$/Si heterojunction can be efficiently enhanced by a transient spike current at 0 V bias when turning on and off the 254 nm UV light. The interface pyroelectric effect of the $ZnGa_2O_4$ film should be responsible for this transient spike photocurrent phenomenon. Our findings in this work pave a feasible way to realize high-performance WBS/Si heterojunction self-powered solar-blind photodetectors.

Solar-blind ultraviolet (UV) photodetectors have drawn much attention due to their extensive applications in civilian and military fields, such as flame detection, environmental monitoring, optical communication, and space research.[1–4] The self-powered solar-blind UV photodetectors can operate without any external power supply, which provides a method to work in unmanned hazardous or harsh environments.[5–8] Generally, self-powered photodetectors can be achieved by the photovoltaic effect of p-n homojunctions, heterojunctions, and Schottky junctions.[9–12] Considering the excellent solar-blind UV photoelectric characteristics of the wide bandgap semiconductor (WBS) and the mature technology of silicon-based materials, WBS/Si heterojunctions should have potential application prospects in the field of self-powered UV detectors and their optoelectronic integrated chips.[13–16] To date, significant progress has been achieved in WBS/Si heterojunction self-powered photodetectors.[17–19] However, most of the reported WBS/Si heterojunction photodetectors have a strong response in the visible light due to the absorption of Si, which in turn leads to poor UV selectivity of the device.[20–22] To solve the above problem, it is necessary to improve the UV response in WBS layer while suppressing the visible light response in Si layer. According to the previous reports, the band structure and interface characteristics in the WBS/Si heterojunction photodetector are the key factors that determine the performance of the device.[23–26] In addition, recent reports suggested that the piezo-phototronic effect and the pyro-phototronic effect can be used to significantly improve the performance of self-powered photodetectors.[27–30] More interestingly, the interface piezoelectric and pyroelectric effects have been demonstrated in centrosymmetric semiconductors, which are free from the symmetry limitation.[31–33]

$ZnGa_2O_4$, with ideal direct wide bandgap (4.4–5.2 eV), excellent structural and thermal stability, has already become one of the most promising materials for solar-blind UV detectors.[34–39] More importantly, the large band offsets of $ZnGa_2O_4$/Si heterojunction

(conduction band offset, $\Delta E_c = 1.74$ eV and valence band offset, $\Delta E_V = 2.34$ eV) would be advantageous to control the electrical transport of carriers in Si layer, thereby suppressing the visible response.[40,41] Therefore, $ZnGa_2O_4$/Si heterojunction should be an ideal structure for the self-powered solar-blind UV photodetection. Moreover, although $ZnGa_2O_4$ has a typical cubic spinel structure, the piezoelectric or pyroelectric effect induced by the symmetry modulation at the heterojunction interfaces is expected to be used to improve the performance of its self-powered heterojunction photodetectors.[31,42] However, there are very few reports on $ZnGa_2O_4$/Si heterojunction photodetector, and the research on its self-powered performance is even blank.[43]

In this work, a self-powered solar-blind UV photodetector has been demonstrated on $ZnGa_2O_4$/Si heterojunction by metal organic chemical vapor deposition (MOCVD). The device exhibits a remarkable rectifying characteristic with a rectification ratio exceeding 10^3 within ± 5 V. At 0 V bias, the peak responsivity occurs at 242 nm with -3 dB cutoff wavelength of $\sim$255 nm, and the UV-visible rejection ratio of our device is $\sim 3 \times 10^2$, suggesting excellent self-powered solar-blind UV detection performance. More interestingly, obvious photocurrent spikes with two different polarities can be observed when the 254 nm UV light is turned on and off at 0 V bias. The pyroelectric effect in the $ZnGa_2O_4$ film may be the main reason for the transient spike, and the detailed mechanism is carefully investigated and discussed. Our findings in this work provide guidance for the design and development of self-powered solar-blind UV photodetectors with high responsivity and quick response speed.

The $ZnGa_2O_4$ films were grown on p-Si (100) substrates by MOCVD (see the supplementary material). After that, the comb-shaped Au Ohmic electrode was fabricated on $ZnGa_2O_4$ by using the photolithography and lift-off technique. Indium (In) was pasted on the back side of the p-Si substrate to serve as the Ohmic electrode on p-Si. Consequently, the $ZnGa_2O_4$/Si heterojunction photodetector was constructed. The samples were characterized by UV-3101PC scanning spectrophotometer, Bruker D8 X-ray diffractometer (XRD) with Cu Kα as the radiation source ($\lambda = 0.154$ nm), and scanning electron microscope (SEM) (HITACHI S-4800). The pyroelectric coefficients of the sample were measured by the pyroelectric attachment of aixACCT TF Analyzer 2000E, Aachen. The current–voltage (I–V) curves and time-dependent photocurrent (I–t) curves were determined by the semiconductor device analyzer (Agilent B1500A). For the photoresponsivity characterization, a 200 W UV-enhanced Xe lamp with a monochromator was used as the light source (see Fig. S1).

The schematic structure of $ZnGa_2O_4$/Si heterojunction photodetector is shown in Fig. 1(a). The comb-shaped Au electrode has a tooth width of 10 μm, a length of 500 μm, and a gap of 10 μm. The quasi-linear I–V relationship indicates that a good Ohmic contact has been formed between Au electrode and $ZnGa_2O_4$ film, and In electrode and the p-Si substrate (see Fig. S2). Figure 1(b) shows the XRD pattern of the $ZnGa_2O_4$ film grown on Si. Besides the (400) diffraction peak of the Si substrate at 69.12°, five diffraction peaks can be clearly observed at 30.26°, 35.69°, 43.34°, 57.42°, and 63.11°, corresponding to (220), (311), (400), (511), and (440) crystal facets of $ZnGa_2O_4$ (JCPDS No. 38–1240), respectively. Figure 1(c) is the SEM surface and cross-sectional images of the $ZnGa_2O_4$ film grown on the Si substrate. The top-view SEM image suggests that the surface of the $ZnGa_2O_4$ film is relatively rough and has obvious large grains. In addition, the thickness of a $ZnGa_2O_4$ film is determined to be about 190 nm using cross-sectional SEM view. Figure 1(d) shows the I–V characteristics of the $ZnGa_2O_4$/Si photodetector in the dark and under the 254 nm UV light illumination with various light intensities of 25, 340, and 1200 μW/cm^2. The I–V curve of the device exhibits a good rectifying behavior in the dark with a rectification ratio exceeding 10^3 within ± 5 V. When the device is illuminated under the 254 nm light, the reversal saturation currents increase monotonously as increasing the power density under each bias voltage.

The time-dependent photoresponse characteristics of the $ZnGa_2O_4$/Si photodetector upon the 254 nm UV illumination are systematically investigated and summarized in Fig. 2(a) by varying the light intensities from 25 to 1200 μW/cm^2 at 0 V bias. Interestingly, an obvious anomalous transient spike current phenomenon with high reproducibility and stability can be observed when turning on and off different intensities of the 254 nm light [see Fig. 2(a)]. Once the device is illuminated with the 254 nm light, a sharp photocurrent peak (I_p) appears immediately and then gradually decays to a steady-state plateau (I_s). After turning off the UV light, another transient spike occurs with reversed polarity (labeled as I_p') and subsequently returns to the initial dark current level (I_d).

Figure 2(b) shows I_p, I_s, and I_p' of the device as a function of the 254 nm light intensity. Obviously, I_p, I_s, and I_p' all monotonically increase with increasing the light intensity. The responsivity is an important parameter to evaluate the performance of a photodetector, which can be calculated by the following formula:[44]

$$R = \frac{I_{photo} - I_{dark}}{PS}, \tag{1}$$

where I_{photo} is the photocurrent, I_{dark} is the dark current, P is the light intensity, and S is the effective area under irradiation. In this work, the transient responsivity R_p and the stable responsivity R_s of the device under the 254 nm illumination with various light intensities were, respectively, determined by the following equations:

$$R_p = \frac{I_p - I_d}{PS}, \tag{2}$$

$$R_s = \frac{I_s - I_d}{PS}. \tag{3}$$

As shown in Fig. 2(c), the stable responsivity R_s remains almost unchanged at around 7.5 mA/W as the light intensity increases. As for the transient responsivity R_p, it decreases from 40.9 to 20 mA/W with increasing the light intensity from 25 to 1200 μW/cm^2. Obviously, the generation of transient spike photocurrent phenomenon significantly enhances the responsivity of the device. Moreover, the responsivity of our device exceeds the responsivity of the most reported WBS/Si heterojunction self-powered solar-blind photodetector.[45,46] Figure 2(d) shows the normalized spectral response of the $ZnGa_2O_4$/Si heterojunction photodetector at 0 V bias with y axis in logarithmic scale. The peak responsivity occurs at 242 nm with a -3 dB cutoff wavelength of 255 nm, suggesting that the device has outstanding intrinsic solar-blind photodetection characteristics. Moreover, the UV-visible rejection ratio of our device ($R_{peak}/R_{400\,nm}$) is $\sim 3 \times 10^2$, which is higher than that of any other reported WBS/Si heterojunction self-powered solar-blind photodetectors.[46]

To further investigate the mechanism of this transient spike current phenomenon, we measure the time-dependent photoresponse characteristics of the device under different wavelengths of light

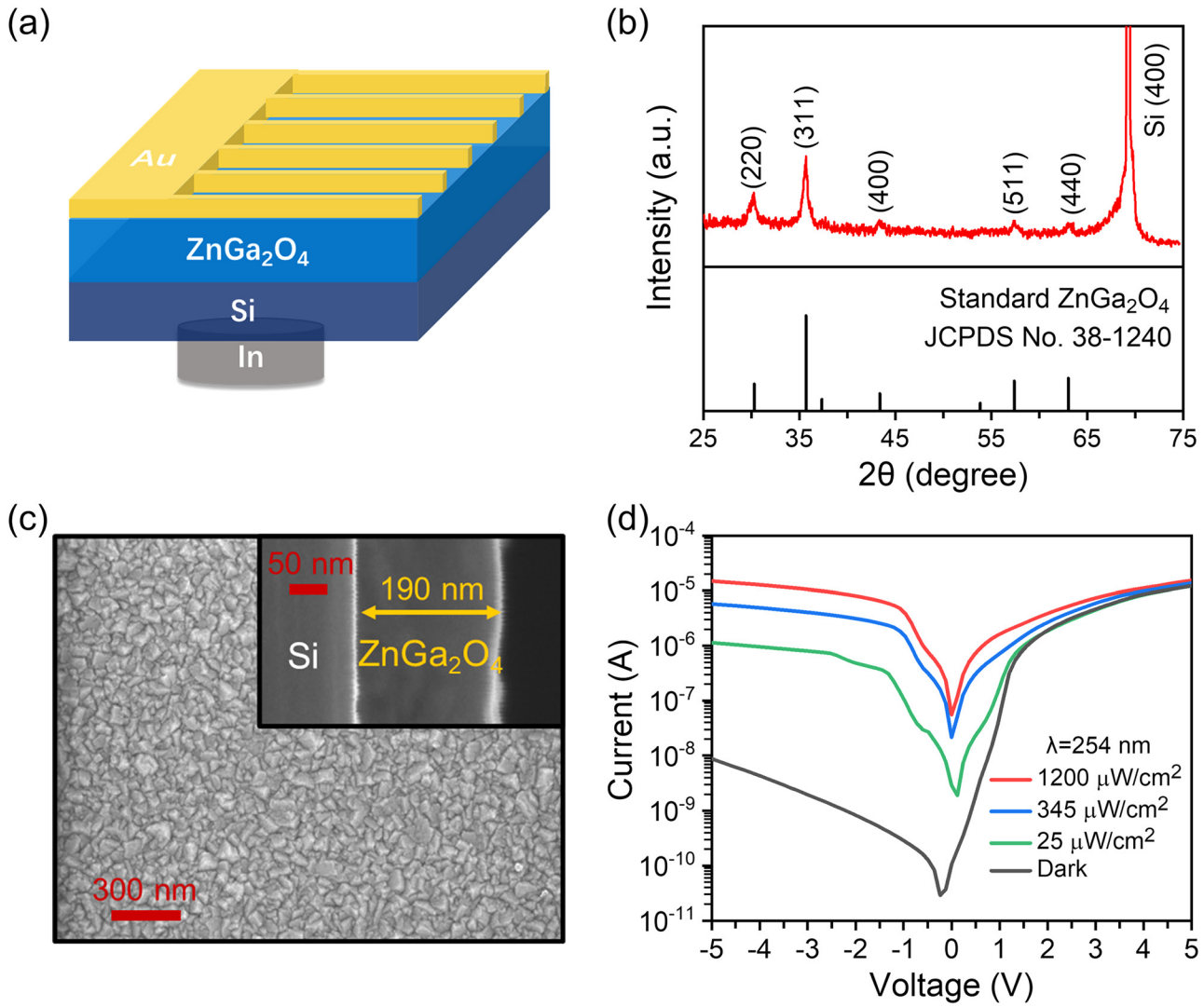

FIG. 1. (a) The schematic structure of $ZnGa_2O_4$/Si photodetector. (b) XRD pattern, (c) SEM surface and cross-sectional images of the $ZnGa_2O_4$ film on the p-Si substrate. (d) *I*–*V* characteristics of the $ZnGa_2O_4$/Si photodetector in the dark and under the 254 nm UV light illumination with various light intensities.

irradiation at 0 V bias as shown in Fig. 3(a). When the incident light wavelength is shorter than 320 nm, the $ZnGa_2O_4$/Si heterojunction photodetector has obvious transient spike current phenomenon. Interestingly, with increasing the incident light wavelength from 320 to 600 nm, the transient spike current phenomenon gradually weakened and finally disappeared completely. From the optical transmission and absorption spectra of $ZnGa_2O_4$ (see Fig. S3) on the transparent *c*-plane sapphire substrate under the same growth conditions as using the p-Si substrate, it can be found that the $ZnGa_2O_4$ film has an average transmittance of ∼90% in the wavelength range of 300–800 nm. Therefore, the generation of transient spike current should be associated with the light absorption in the $ZnGa_2O_4$ layer.

To understand the transient spike current phenomenon and the photoresponse property of $ZnGa_2O_4$/Si photodetector, the energy band diagram of $ZnGa_2O_4$/Si heterojunction is given in Fig. 3(b). The band offsets are determined as $\Delta E_c = 1.74$ eV and $\Delta E_V = 2.34$ eV using the electron affinity of 4.05 and 2.31 eV, and band gap of 1.12 and 5.20 eV for p-Si and $ZnGa_2O_4$, respectively.[40,41] Under the 240 nm illumination, the electron–hole pairs would be excited in $ZnGa_2O_4$ layer and rapidly separated by the built-in electric field under zero bias. The electrons transport toward n-$ZnGa_2O_4$, and the holes transport toward p-Si. However, for the 600 nm illumination, it is not able to excite the carriers in n-$ZnGa_2O_4$, but can be absorbed by p-Si. The energy band diagram of the $ZnGa_2O_4$/Si heterojunction under the 600 nm light illumination at 0 V bias is shown in Fig. S4. Due to the large band offsets, the photogenerated carriers in p-Si were efficiently blocked and cannot contribute to the photocurrent. In this case, the visible light response from the Si substrate is efficiently suppressed, resulting in a high UV-visible rejection ratio. Additionally, since the obvious current spike phenomenon occurs only when switching light

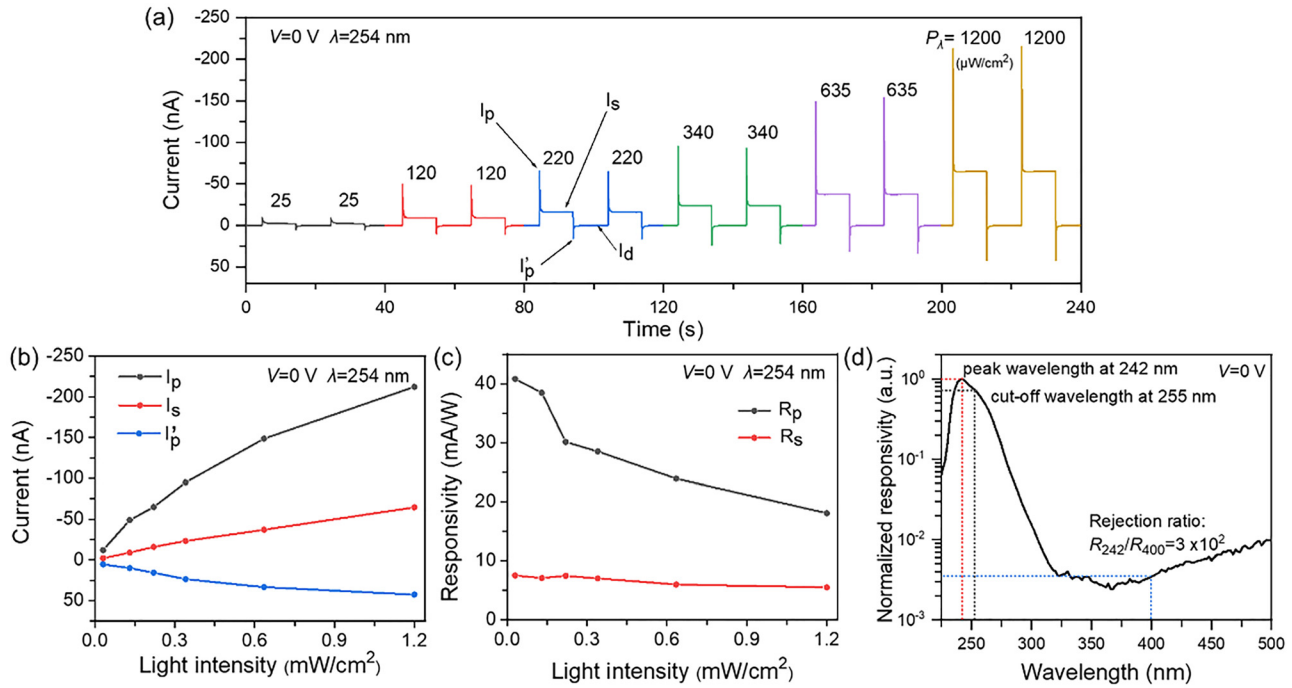

FIG. 2. (a) Time-dependent photoresponse characteristics of the $ZnGa_2O_4$/Si photodetector under the 254 nm illumination with different light intensities from 25 to 1200 μW/cm^2 at 0 V bias. (b) I_p, I_s, and I'_p of the device as a function of the 254 nm light intensity. (c) Transient responsivity and stable responsivity of the device as a function of the 254 nm light intensity. (d) Normalized spectral response of the $ZnGa_2O_4$/Si photodetector with y axis in logarithmic scale.

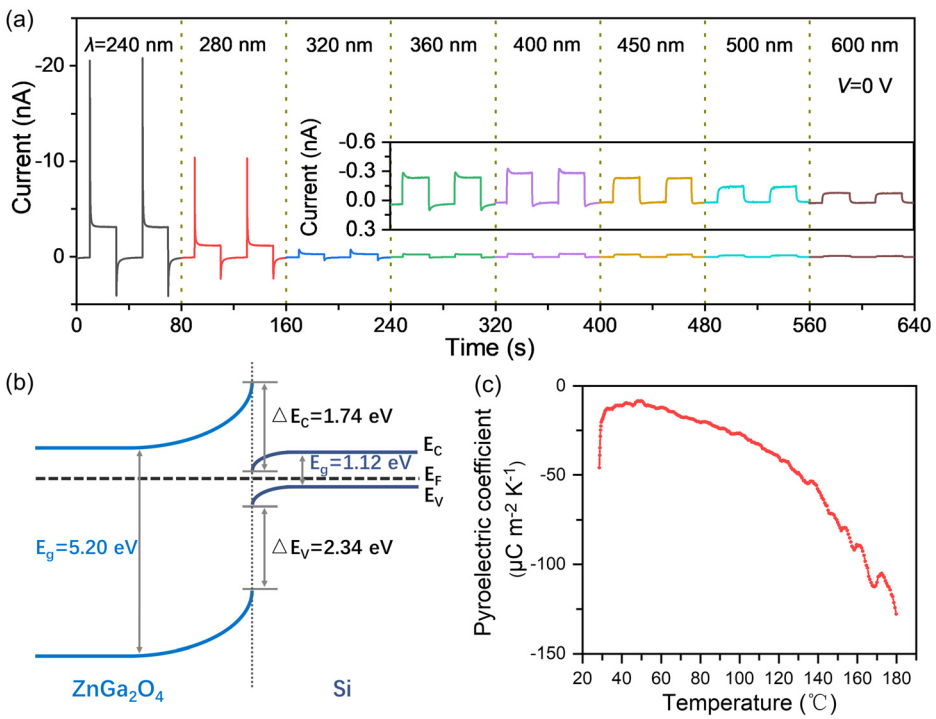

FIG. 3. (a) Time-dependent photoresponse characteristics of the $ZnGa_2O_4$/Si photodetector under different incident light wavelengths at 0 V bias. (b) Schematic energy band diagram of the $ZnGa_2O_4$/Si heterojunction. (c) Temperature dependence of pyroelectric coefficients of $ZnGa_2O_4$/Si heterojunction from room temperature to 180 °C.

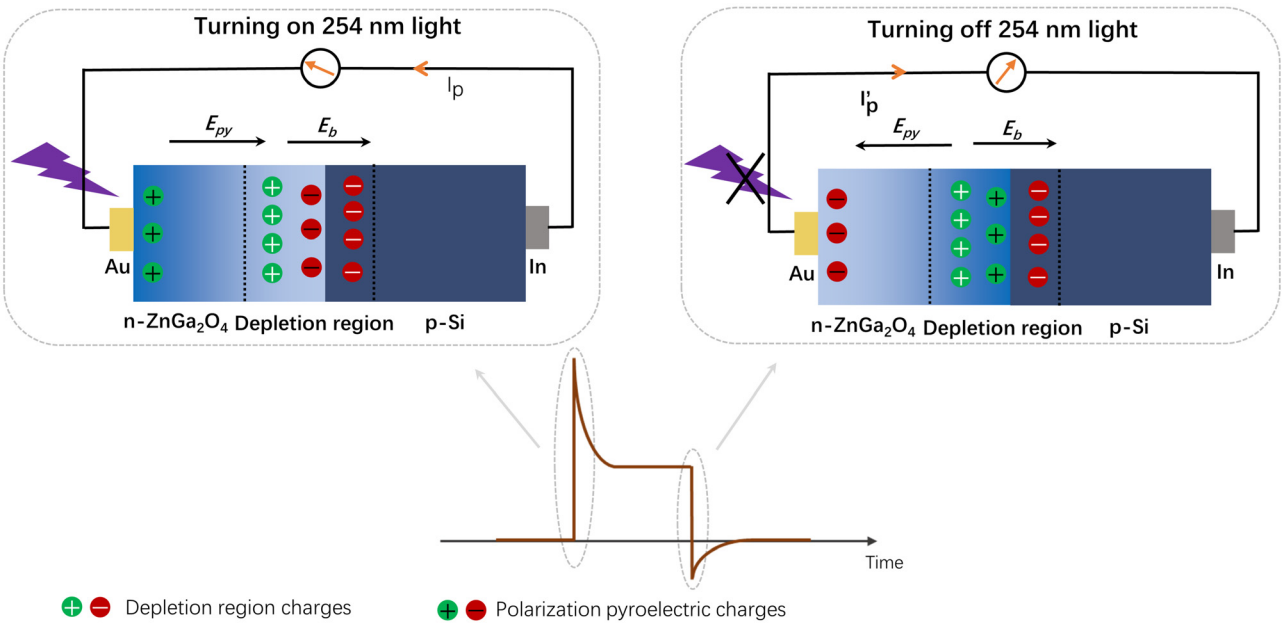

FIG. 4. The mechanism of transient spike current in the $ZnGa_2O_4$/Si photodetector.

with a wavelength less than 280 nm [see Fig. 3(a)], the spike process should be related to the photoresponse in n-$ZnGa_2O_4$ layer. According to the previous reports, the transient spike current phenomenon was commonly observed in the self-powered photodetectors based on noncentrosymmetric semiconductor materials (such as ZnO, CdS, SnS, and $BaTiO_3$) by pyro-phototronic and piezo-phototronic effects.[27–30,47] Although $ZnGa_2O_4$ has a typical cubic spinel structure, the symmetry modulation at the heterojunction interface can also lead to the polarization in the semiconductors and generates substantial piezoelectric and pyroelectric effects.[31–33,48] Figure 3(c) presents the temperature dependence of pyroelectric coefficients of the sample from room temperature to 180 °C. The pyroelectric effect can be clearly observed with a pyroelectric coefficient of 45.9 $\mu C\ m^{-2}\ K^{-1}$ at room temperature. Therefore, the transient spike current phenomenon of the $ZnGa_2O_4$/Si photodetector should be attributed to the interface pyroelectric effect of the $ZnGa_2O_4$ film.

To analyze the mechanism of transient spike current in the $ZnGa_2O_4$/Si self-powered photodetector, schematic diagrams of the related processes are presented in Fig. 4. When turning on the 254 nm light, photons are mainly absorbed by the $ZnGa_2O_4$ layer, and the photogenerated carriers are separated under the built-in electric field (E_b). Since the direction of the built-in electric field points from n-$ZnGa_2O_4$ to p-Si, the electrons move toward n-$ZnGa_2O_4$ and the holes move toward p-Si. Meanwhile, an instantaneous temperature increase inside $ZnGa_2O_4$ would be induced when turning on the 254 nm UV illumination, and the temperature difference could lead to a distribution of polarization pyroelectric charges and a corresponding pyroelectric potential (E_{py}).[28–30] The direction of the pyroelectric

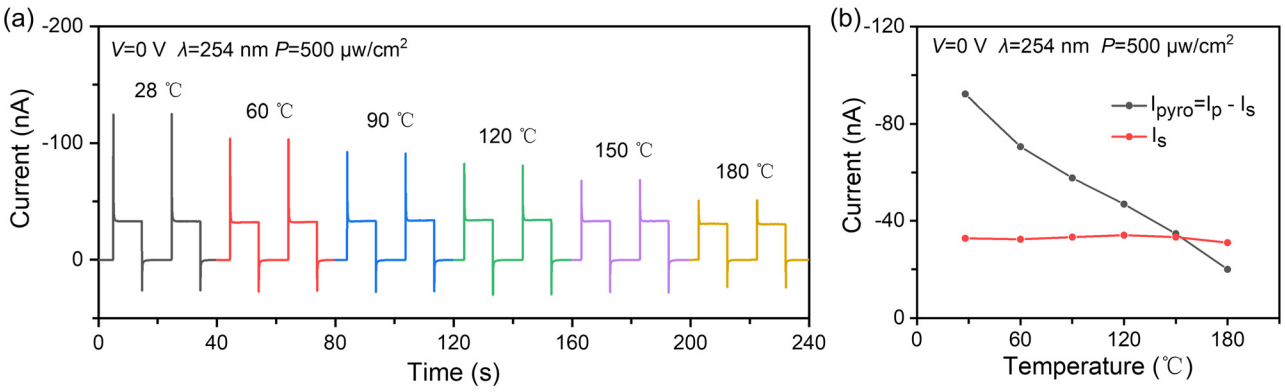

FIG. 5. (a) Time-dependent photoresponse characteristics of the $ZnGa_2O_4$/Si photodetector under the 254 nm illumination with different background ambient temperatures at 0 V bias. (b) I_{pyro} and I_s of the device under the 254 nm illumination as a function of background ambient temperature at 0 V bias.

potential (E_{py}) is the same as the direction of the built-in electric field.[28,47] Therefore, the photocurrent shows a rapidly rising spike process, and the peak current I_p is the sum of photocurrent (I_{ph}) and pyrocurrent (I_{pyro}). As the 254 nm light continues to irradiate, the temperature inside $ZnGa_2O_4$ tends to be the same, and the pyroelectric potential (E_{py}), thus disappears. Therefore, the current quickly decreases and reaches a steady state I_s, which can be considered as the net photocurrent. The pyrocurrent I_{pyro} could be calculated by $I_{pyro} = I_p - I_s$. Once the 254 nm UV light is turned off, the reverse pyroelectric potential (E_{py}) would be formed due to an instantaneous temperature decrease, and thus a transient spike current in the opposite direction can be observed.[28,47] After that, it returns to the steady-state dark current.

To further verify the influence of the background ambient temperature on the transient spike current, we have studied the *I*–*t* characteristic curves of the device under different background ambient temperatures. Figure 5(a) shows the time-dependent photoresponse characteristics of the $ZnGa_2O_4$/Si photodetector under the 254 nm illumination with different background ambient temperatures at 0 V bias. For the background ambient temperature varying from 28 °C to 180 °C, an obvious spike current phenomenon with high reproducibility and stability can be observed when turning on and off the 254 nm light. In addition, as shown in Fig. 5(b), the pyrocurrent I_{pyro} gradually decreases with increasing the background temperature, which can be explained by the improved rate of temperature change at low temperature.[49] However, there is almost no change in the steady-state photocurrent I_s,

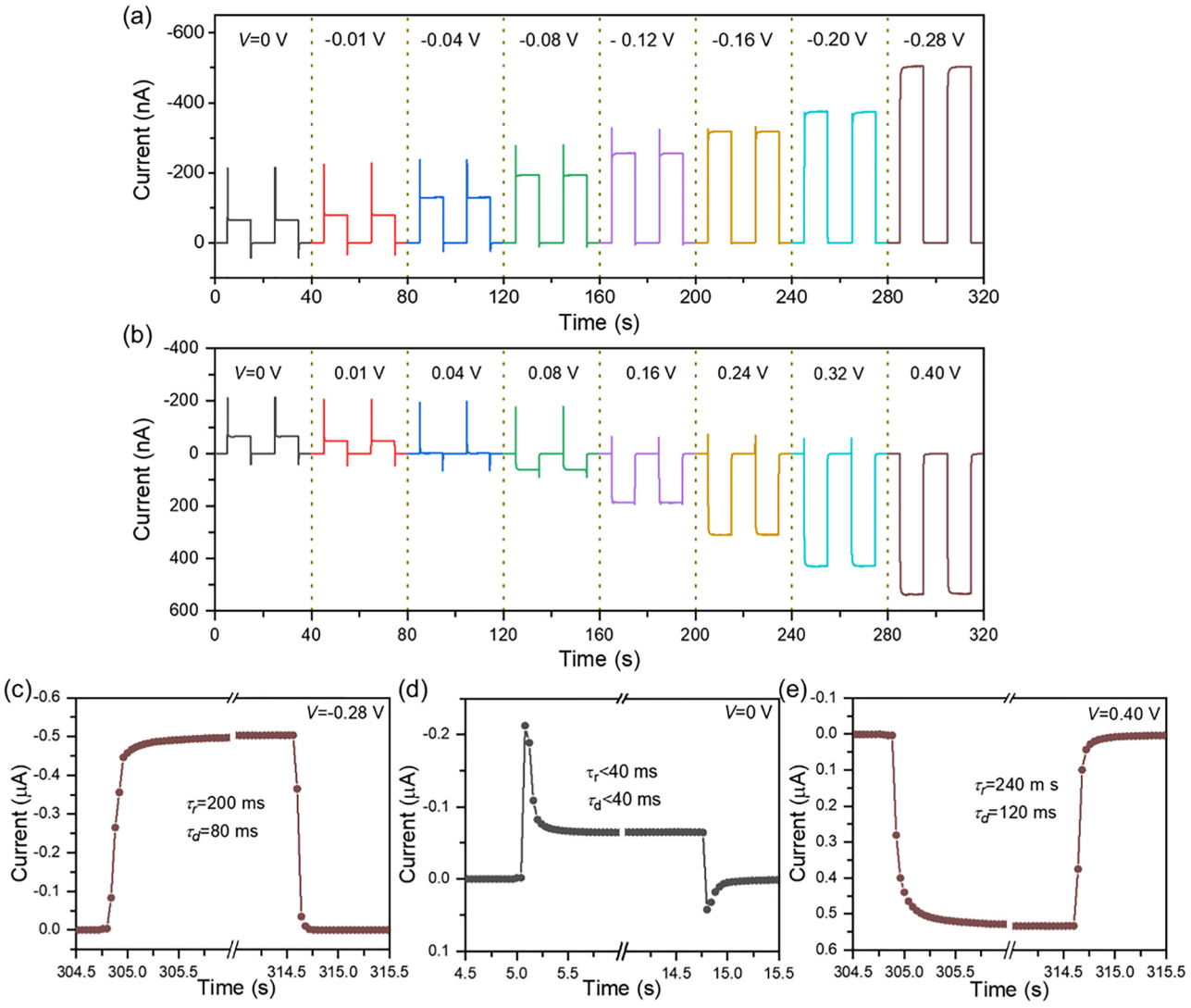

FIG. 6. Time-dependent photoresponse characteristics of the $ZnGa_2O_4$/Si photodetector under the 254 nm illumination with 1200 $\mu W/cm^2$ intensity at different bias voltages from 0 to −0.28 V (a) and from 0 to 0.40 V (b). The enlarged views of the rise and decay edges of the device at different external bias voltages: −0.28 V (c), 0 V (d), and 0.40 V (e).

that is, the net photocurrent has no temperature dependence. These results further verify that the transient spike current phenomenon originates from the pyroelectric effect in the $ZnGa_2O_4$ film.

Figure 6 shows the time-dependent photoresponse of the $ZnGa_2O_4$/Si photodetector under different applied potentials. When a small bias is applied to the device (both forward bias and reverse bias), the spike current phenomenon can still be observed. Interestingly, the direction of the transient spike photocurrent does not change with the direction of the applied bias when turning on the 254 nm light. The steady-state photocurrent and steady-state dark current are close to zero at 0.04 V and only transient spike current can be observed, which has great application potential in the fast binary response of high-frequency devices and optical communication.[50,51] However, as the bias voltage increases, the transient spike current phenomenon gradually disappears due to the compensation of pyroelectric effect by joule heating.[30,52] To study the relationship between transient spike phenomenon and response speed of the device, the enlarged views of the rise and decay edges of the device at different external bias voltages of −0.28, 0, and 0.40 V are shown in Figs. 6(c)–6(e), respectively. The rise time (τ_r) and decay time (τ_d) are defined as the time for the photocurrent from 10% to 90% and from 90% to 10% of the maximum value, respectively. At 0 V bias, both the rise time and decay time of the device were shorter than 40 ms (the detection limit). However, the rise/decay times of the device at −0.28 and 0.40 V were 200/80 and 240/120 ms, respectively. Obviously, the transient spike phenomenon under 0 V bias improves the response speed of the device, which also further confirming that the fast response of the $ZnGa_2O_4$/Si photodetector is mainly derived from the pyroelectric effect in the $ZnGa_2O_4$ film.[28,53,54] Moreover, the spike-like transient open-circuit voltage can be also observed for the $ZnGa_2O_4$/Si photodetector by periodically switching on and off the 254 nm UV light (see Fig. S5). Obviously, the spike could efficiently improve the output current/voltage and the response speed. Our findings in this work provide guidance for the design and development of corresponding optoelectronics for ultrafast photosensing and high efficiency power generators.

In summary, we prepared a $ZnGa_2O_4$ film on the p-Si (100) substrate and constructed the $ZnGa_2O_4$/Si self-powered solar-blind photodetector. The *I*–*V* curve of the device exhibits an obvious rectifying characteristic with a rectification ratio of more than 10^3 at ±5 V. At 0 V bias, the peak responsivity occurs at 242 nm with −3 dB cutoff wavelength of ∼255 nm, and the UV-visible rejection ratio is $\sim 3 \times 10^2$, suggesting the excellent self-powered solar-blind UV detection performance. More interestingly, an anomalous transient spike current phenomenon with high reproducibility can be clearly observed at 0 V bias when turning on and off the 254 nm light due to the interface pyroelectric effect of the $ZnGa_2O_4$ film. Both the rise time and decay time of the device were shorter than 40 ms (the detection limit). The spike in transient photocurrent could efficiently improve the responsivity and the response speed of the device. Our work provides a feasible method for realizing high-performance WBS/Si heterojunction self-powered solar-blind photodetectors.

See the supplementary material for the preparation of $ZnGa_2O_4$ films, spectrum of the light source, *I*–*V* characteristics of the Au–$ZnGa_2O_4$–Au and In–Si–In, optical transmission and absorption spectra of the $ZnGa_2O_4$ film grown on *c*-plane sapphire, the energy band diagram of the $ZnGa_2O_4$/Si heterojunction under the 600 nm light illumination at 0 V bias and open-circuit voltage transient characteristics of the $ZnGa_2O_4$/Si heterojunction under the 254 nm illumination.

This work was supported by the National Natural Science Foundation of China (Nos. 62074148, 61875194, 11727902, 12074372, 11774341, 11974344, 61975204, and 11804335), the 100 Talents Program of the Chinese Academy of Sciences, Youth Innovation Promotion Association, CAS (No. 2020225), and Open Project of the State Key Laboratory of Luminescence and Applications (Nos. SKLA-2020-02 and SKLA-2020-06).

DATA AVAILABILITY

The data that support the findings of this study are available from the corresponding authors upon reasonable request.

REFERENCES

[1]C. Wu, L. Qiu, S. Li, D. Guo, P. Li, S. Wang, P. Du, Z. Chen, A. Liu, X. Wang, H. Wu, F. Wu, and W. Tang, Mater. Today Phys. **17**, 100335 (2021).
[2]C. Xie, X.-T. Lu, X.-W. Tong, Z.-X. Zhang, F.-X. Liang, L. Liang, L.-B. Luo, and Y.-C. Wu, Adv. Funct. Mater. **29**, 1806006 (2019).
[3]L. X. Qian, H. Y. Liu, H. F. Zhang, Z. H. Wu, and W. L. Zhang, Appl. Phys. Lett. **114**, 113506 (2019).
[4]Y. Xu, X. Chen, Y. Zhang, F. Ren, S. Gu, and J. Ye, IEEE Electron Device Lett. **41**, 1617 (2020).
[5]Y. C. Chen, Y. J. Lu, C. N. Lin, Y. Z. Tian, C. J. Gao, L. Dong, and C. X. Shan, J. Mater. Chem. C **6**, 5727 (2018).
[6]L. Su, W. Yang, J. Cai, H. Chen, and X. Fang, Small **13**(45), 1701687 (2017).
[7]R. R. Zhuo, D. Wu, Y. G. Wang, E. P. Wu, C. Jia, Z. F. Shi, T. T. Xu, Y. T. Tian, and X. J. Li, J. Mater. Chem. C **6**, 10982 (2018).
[8]S. Mitra, Y. Pak, B. Xin, D. R. Almalawi, N. Wehbe, and I. S. Roqan, ACS Appl. Mater. Interfaces **11**, 38921 (2019).
[9]Y. Ning, Z. M. Zhang, F. Teng, and X. S. Fang, Small **14**, 1703754 (2018).
[10]Y. Zhu, K. Liu, Q. Ai, Q. Hou, X. Chen, Z. Zhang, X. Xie, B. Li, and D. Shen, J. Mater. Chem. C **8**, 2719 (2020).
[11]X. Chen, K. W. Liu, Z. Z. Zhang, C. R. Wang, B. H. Li, H. F. Zhao, D. X. Zhao, and D. Z. Shen, ACS Appl. Mater. Interfaces **8**, 4185 (2016).
[12]S. Mitra, Y. Pak, N. Alaal, M. N. Hedhili, D. R. Almalawi, N. Alwadai, K. Loganathan, Y. Kumarasan, N. Lim, G. Y. Jung, and I. S. Roqan, Adv. Opt. Mater. **7**, 21 (2019).
[13]J. Michel, J. F. Liu, and L. C. Kimerling, Nat. Photonics **4**, 527 (2010).
[14]L. Wang, J. S. Jie, Z. B. Shao, Q. Zhang, X. H. Zhang, Y. M. Wang, Z. Sun, and S. T. Lee, Adv. Funct. Mater. **25**, 2910 (2015).
[15]T. Ji, Q. Liu, R. J. Zou, Y. G. Sun, K. B. Xu, L. W. Sang, M. Y. Liao, Y. Koide, L. Yu, and J. Q. Hu, Adv. Funct. Mater. **26**, 1400 (2016).
[16]C. H. Kang, I. Dursun, G. Liu, L. Sinatra, X. Sun, M. Kong, J. Pan, P. Maity, E.-N. Ooi, T. K. Ng, O. F. Mohammed, O. M. Bakr, and B. S. Ooi, Light: Sci. Appl. **8**, 94 (2019).
[17]Z. Hou, G. Li, C. Ling, H. Wang, L. Zhu, T. Guo, T. Zhang, B. Feng, M. Cao, and Q. Xue, Adv. Electron. Mater. **6**, 2000501 (2020).
[18]N. Prakash, G. Kumar, M. Singh, A. Barvat, P. Pal, S. P. Singh, H. K. Singh, and S. P. Khanna, Adv. Opt. Mater. **6**, 1800191 (2018).
[19]W. Gao, Z. Zheng, L. Huang, J. Yao, Y. Zhao, Y. Xiao, and J. Li, ACS Appl. Mater. Interfaces **11**, 40222 (2019).
[20]K. B. Ko, B. D. Ryu, M. Han, C.-H. Hong, T. A. Doan, and T. V. Cuong, J. Alloys Compd. **823**, 153884 (2020).
[21]T. C. Zhang, Y. Guo, Z. X. Mei, C. Z. Gu, and X. L. Du, Appl. Phys. Lett. **94**, 113508 (2009).
[22]J.-D. Hwang, D.-H. Wu, and S.-B. Hwang, IEEE Photonics Technol. Lett. **26**, 1081 (2014).
[23]Y. N. Hou, Z. X. Mei, H. L. Liang, D. Q. Ye, S. Liang, C. Z. Gu, and X. L. Du, Appl. Phys. Lett. **98**, 263501 (2011).
[24]Z. Liang, P. Zeng, P. Liu, C. Zhao, W. Xie, and W. Mai, ACS Appl. Mater. Interfaces **8**, 19158 (2016).

[25]X. Li, M. Zhu, M. Du, Z. Lv, L. Zhang, Y. Li, Y. Yang, T. Yang, X. Li, K. Wang, H. Zhu, and Y. Fang, Small **12**, 595 (2016).
[26]C.-Y. Huang, Y.-J. Yang, J.-Y. Chen, C.-H. Wang, Y.-F. Chen, L.-S. Hong, C.-S. Liu, and C.-Y. Wu, Appl. Phys. Lett. **97**, 013503 (2010).
[27]X. Hu, X. Li, G. Li, T. Ji, F. Ai, J. Wu, E. Ha, and J. Hu, Adv. Funct. Mater. **8**, 2011284 (2021).
[28]Z. N. Wang, R. M. Yu, C. F. Pan, Z. L. Li, J. Yang, F. Yi, and Z. L. Wang, Nat. Commun. **6**, 8401 (2015).
[29]W. B. Peng, R. M. Yu, X. F. Wang, Z. N. Wang, H. Y. Zou, Y. N. He, and Z. L. Wang, Nano Res. **9**, 3695 (2016).
[30]Y. Dai, X. Wang, W. Peng, C. Xu, C. Wu, K. Dong, R. Liu, and Z. L. Wang, Adv. Mater. **30**, 1705893 (2018).
[31]M. M. Yang, Z. D. Luo, Z. Mi, J. Zhao, S. P. E, and M. Alexe, Nature **584**, 377 (2020).
[32]E. Meirzadeh, D. V. Christensen, E. Makagon, H. Cohen, I. Rosenhek-Goldian, E. H. Morales, A. Bhowmik, J. M. G. Lastra, A. M. Rappe, D. Ehre, M. Lahav, N. Pryds, and I. Lubomirsky, Adv. Mater. **31**, 1904733 (2019).
[33]J. Ding, J. Cheng, F. Dogan, Y. Li, W. Lin, Y. Yao, A. Manchon, K. Yang, and T. Wu, ACS Appl. Mater. Interfaces **12**, 42982 (2020).
[34]Z. Galazka, S. Ganschow, R. Schewski, K. Irmscher, D. Klimm, A. Kwasniewski, M. Pietsch, A. Fiedler, I. Schulze-Jonack, M. Albrecht, T. Schroder, and M. Bickermann, APL Mater. **7**, 011301 (2019).
[35]R. H. Huang, C. Y. Huang, S. L. Ou, T. K. Juang, and P. L. Liu, Cryst. Growth Des. **17**, 6071 (2017).
[36]S. H. Tsai, S. Basu, C. Y. Huang, L. C. Hsu, Y. G. Lin, and R. H. Horng, Sci. Rep. **8**, 14056 (2018).
[37]D. Han, K. Liu, Q. Hou, X. Chen, J. Yang, B. Li, Z. Zhang, L. Liu, and D. Shen, Sens. Actuator, A **315**, 112354 (2020).
[38]J. Boy, M. Handwerg, R. Mitdank, Z. Galazka, and S. F. Fischer, AIP Adv. **10**, 055005 (2020).
[39]M. I. Chen, A. K. Singh, J. L. Chiang, R. H. Horng, and D. S. Wuu, Nanomaterials **10**, 2208 (2020).
[40]Y.-C. Shen, C.-Y. Tung, C.-Y. Huang, Y.-C. Lin, Y.-G. Lin, and R.-H. Horng, ACS Appl. Electron. Mater. **1**, 783 (2019).
[41]X. H. Xie, Z. Z. Zhang, C. X. Shan, H. Y. Chen, and D. Z. Shen, Appl. Phys. Lett. **101**, 081104 (2012).
[42]D. Gogoi, A. A. Hussain, S. Biswasi, and A. R. Pal, J. Mater. Chem. C **8**, 6450–6460 (2020).
[43]W. Lin, D. Zhang, S. Liu, Y. Li, W. Zheng, and F. Huang, Mater. Lett. **283**, 128805 (2021).
[44]Z. Cheng, K. W. Liu, J. L. Yang, X. Chen, X. H. Xie, B. H. Li, Z. Z. Zhang, L. Liu, C. X. Shan, and D. Z. Shen, ACS Appl. Mater. Interfaces **11**, 34144 (2019).
[45]A. Atilgan, A. Yildiz, U. Harmanci, M. T. Gulluoglu, and K. Salimi, Mater. Today Commun. **24**, 101105 (2020).
[46]C. Yang, X. M. Li, W. D. Yu, X. D. Gao, X. Cao, and Y. Z. Li, J. Phys. D **42**, 152002 (2009).
[47]M. Kumar, M. Patel, J. Kim, and D. Lim, Nanoscale **9**, 19201 (2017).
[48]S. Yuan, W. F. Io, J. Mao, Y. Chen, X. Luo, and J. Hao, ACS Appl. Nano Mater. **3**, 11979 (2020).
[49]Y. Chang, J. Wang, F. Wu, W. Tian, and W. Zhai, Adv. Funct. Mater. **30**, 2001450 (2020).
[50]K. Hu, F. Teng, L. Zheng, P. Yu, Z. Zhang, H. Chen, and X. Fang, Laser Photonics Rev. **11**, 1600257 (2017).
[51]S. Dalgleish, M. M. Matsushita, L. Hu, B. Li, H. Yoshikawa, and K. Awaga, J. Am. Chem. Soc. **134**, 12742 (2012).
[52]Z. N. Wang, R. M. Yu, X. F. Wang, W. Z. Wu, and Z. L. Wang, Adv. Mater. **28**, 6880 (2016).
[53]A. K. Rana, M. Kumar, D. K. Ban, C. P. Wong, J. Yi, and J. Kim, Adv. Electron. Mater. **5**, 1900438 (2019).
[54]M. Kumar, M. Patel, T. T. Nguyen, J. Kim, and J. Yi, Nanoscale **10**, 6928 (2018).